

NANOCOMPOSITES OF ZINC OXIDE ON GRAPHENE OXIDE: A RAPID REDUCTION OF GRAPHENE OXIDE

M. A. GOMEZ-ALVAREZ, A. DIAZ, I. MOTA, V. CABRERA, L. RESÉNDIZ*
Instituto Politécnico Nacional, Section of Postgraduate Studies and Research, Mexico City, 07340, Mexico

In this work, graphene oxide (GO) and ZnO were synthesized using the modified Hummers method and the Spanhel and Anderson method, respectively. ZnO/GO composites were then successfully synthesized using a fast and direct process. The results of the X-ray diffraction, scanning electron microscopy (SEM), Raman spectroscopy, and Fourier-transform infrared spectroscopy (FTIR) proved the conversion of GO to reduced graphene oxide, without additional chemical agents or processing at high temperatures and under high vacuum. This study reveals the interaction between oxide materials, which can be of help in the field of electronic microdevice manufacturing.

(Received July 28, 2020; Accepted January 19, 2021)

Keywords: Graphene oxide, Zinc oxide, ZnO/GO composites

1. Introduction

Graphene oxide (GO) is an important material in solid-state physics because of its high transparency and flexibility [1]. The functional groups in GO, which are obtained during the oxidation of graphite powder, allow it to be dispersed in several solutions. This property facilitates its deposition by simple chemical methods such as drop casting [2], spin coating [3], spray pyrolysis [4], and Langmuir–Blodgett [5].

ZnO is a wide-bandgap semiconductor (3.3 eV) with a large exciton binding energy (60 meV) [6], [7]. In addition, ZnO is inexpensive because it can be synthesized by several chemical methods such as hydrothermal synthesis [8], Spanhel and Anderson method [9], sol-gel method [10], and green synthesis [11]. ZnO thin films have been extensively studied due to their potential applications in electronic microdevices such as thin film transistors (TFTs) [12], photodiodes [13], solar cells [14], and gas sensors [15].

Several studies have investigated GO reduction. Thomas N. Blanton et al. studied the conversion of GO to rGO due to exposure to high energy X-rays under an He atmosphere [16]. Different thermal and chemical treatments were used for decreasing the oxygen content in GO films [17], [18], [19]. Au/ZnO/GO nanocomposites fabricated by a spray coating method exhibited good photocatalytic reduction of graphene oxide [20]. Typically, chemical modification of GO requires controlled conditions such as high vacuum; high temperatures, which also enhance the physical–chemical alteration of the substrate; and chemical agents that leave residues after their removal, which affects the original properties of the material.

In this work, GO and ZnO were prepared using the modified Hummers method and Spanhel and Anderson method, respectively. Different volumes of ZnO suspension were then mixed with the GO powder. A simple thermal process was used to remove the solvent and obtain ZnO/GO nanocomposites. ZnO, GO, and ZnO/GO nanocomposites were characterized by X-ray diffraction (XRD), scanning electron microscopy (SEM), Raman spectroscopy, and Fourier-transform infrared spectroscopy (FTIR). The characterization results of the nanocomposites demonstrate that this simple method can eliminate the oxygenated species of GO without chemical agents or high synthesis temperatures.

* Corresponding author: lresendiz@ipn.mx

2. Experimental details

GO powder was synthesized using the modified Hummers method [21], graphite (2 g) and sodium nitrate (NaNO_3 , 1 g) were mixed into an ice-mounted beaker. Next, sulfuric acid (H_2SO_4 , 100 ml) was slowly added, maintaining the mixture under constant stirring at 600 rpm. Potassium permanganate (KMnO_4 , 6 g) was then slowly added for 30 min. Deionized water (DIW, 300 ml) was gradually added, and the solution was kept under magnetic stirring at 700 rpm for 2 h at 15 °C. Finally, hydrogen peroxide (H_2O_2 , 160 ml) was added at 750 rpm for 15 min at 15 °C. GO purification was carried out for eliminating some ions, precursors, and remnants of the chemical reaction to enhance the material purity. This process involved the filtration of the liquid phase of GO by placing the material in a 5 μm pore size Teflon membrane connected to a vacuum pump to obtain GO dark paste. This was followed by 3 washes with 3 solutions: H_2SO_4 (5% vol.), H_2O_2 (5% vol.), and hydrochloric acid (HCl, 1 molar).

ZnO suspension was synthesized using the Spanhel and Anderson method [22], in which ethanol ($\text{C}_2\text{H}_5\text{OH}$, 50 ml) was added to a beaker and gradually mixed with zinc acetate dihydrate ($\text{Zn}(\text{CH}_3\text{COO})_2 \cdot 2\text{H}_2\text{O}$, 1.1 g), maintaining the solution at 80 °C under magnetic stirring at 200 rpm for 10 min, precisely at this step the reaction takes place and the growth of the nanoparticles begins. Subsequently, the solution was placed on ice to cool at approximately 15 °C. Separately, ethanol ($\text{C}_2\text{H}_5\text{OH}$, 50 ml) was added to a beaker and mixed with lithium hydroxide ($\text{LiOH} \cdot \text{H}_2\text{O}$, 0.29 g), maintaining the solution under ultrasonic stirring for 15 min. This solution was also placed on ice to cool at approximately 15 °C. The $\text{C}_2\text{H}_5\text{OH}$ and $\text{LiOH} \cdot \text{H}_2\text{O}$ solution was added dropwise for 30 min to the $\text{C}_2\text{H}_5\text{OH}$ and $\text{Zn}(\text{CH}_3\text{COO})_2 \cdot 2\text{H}_2\text{O}$ solution to stop the reaction and prevent the excessive growth of nanoparticles. The ZnO nanoparticles were kept at approximately 15 °C to avoid agglomeration.

ZnO/GO composites were obtained following this simple procedure: ZnO (3.5 ml) and GO (61 mg) were mixed to obtain the first sample called composite 1. The second sample (composite 2) was obtained by mixing ZnO (4 ml) and GO (61 mg). The last sample (composite 3) was obtained by mixing ZnO (5 ml) and GO (61 mg). The samples were stirred under ultrasonic agitation for 10 min. Finally, composites were subjected to heat treatment at 100 °C for 20 min under air atmosphere to evaporate the solvent.

XRD characterizations were carried out on a Rigaku Ultima III spectrometer ($\text{Cu-K}_\alpha = 0.1542 \text{ nm}$). SEM characterizations were carried out using a Jeol (JSM-6610LV). Raman measurements were conducted on a Horiba Jobin Yvon (LabRAM HR-800) with laser excitation at 532 nm, incident laser power of 1 mW, and 100x objective lens ($\text{NA} = 0.9$). FTIR measurements were obtained with a Bruker (Vertex 70).

3. Results and discussion

Fig. 1a) shows the diffractogram corresponding to the as-prepared GO. The characteristic peak of GO was observed at $2\theta = 10.6^\circ$, corresponding to the (001) plane. These results agree with the literature, which indicates that the characteristic diffraction peak of GO occurs at $2\theta = 7^\circ - 12^\circ$ [23]. In addition, the characteristic peaks of graphite were also observed at $2\theta = 26.5^\circ$ and 42.5° , corresponding to the (002) and (101) planes, respectively [24].

Fig. 1b) shows the diffractogram of ZnO. The main peaks were observed at $2\theta = 31.7^\circ$, 34.4° , and 36.2° , which corresponds to the (100), (002), and (101) planes, respectively [25]. The zinc oxide particles were found to have a wurtzite spatial configuration and a hexagonal close packed crystal structure (HCP) [26].

Fig. 1c) shows the diffractograms of the ZnO/GO composites. The characteristic GO peak could not be observed and a very wide peak occurred at $2\theta = 24.8^\circ$, corresponding to the reduced graphene oxide (r-GO). This absence of the GO peak suggests that the r-GO leaves remained disorderly packaged despite their strong π - π interaction. Possibly the excitonic generation increases, resulting in the formation of sp^2 hybrid domains, giving r-GO the appearance of graphene. As a result, the intensity of the r-GO peaks also increases with the concentration of ZnO in the composites. These results prove the conversion of GO to rGO in the synthesized

nanocomposites. Since the chemical composition of GO remains stable up to a temperature of 520 °C at atmospheric pressure [27], thermal treatment of the composites did not affect the reduction in the GO oxygen content, which was directly due to the incorporation of ZnO.

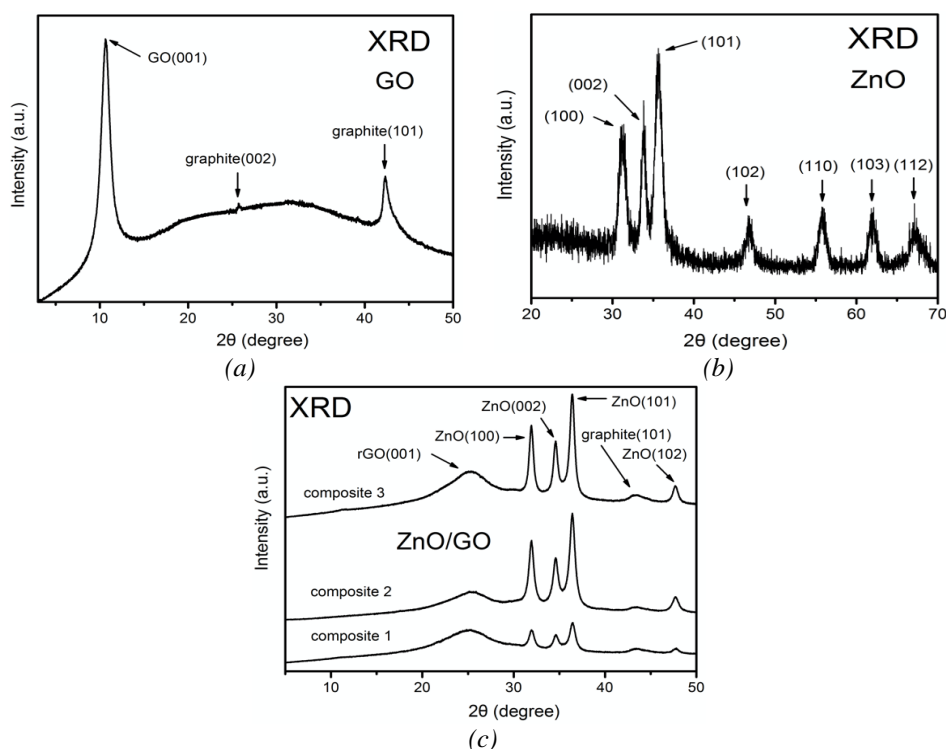


Fig. 1. XRD spectra of a) GO, b) ZnO and c) ZnO/GO composites.

Fig. 2a) shows the topography of GO. GO appears as flakes or sheets with folded and wrinkled undulations characteristic of this material. Even the edges of the GO sheets were bent in laugh-like structures. In addition, GO sheets were found to have highly porous nanostructures. The GO sheets wrinkle due to the interaction between the adjacent sheets that form the material. As a result, they tend to deform in the presence of carboxyl group (C–OH) edges that create “peak and valley” undulations in the edge-to-edge interaction sites.

Fig. 2 b) shows the SEM image of ZnO nanoparticles, which revealed that the particle size was 41 nm. In addition, the nanoparticles were uniformly dispersed, presenting random shapes.

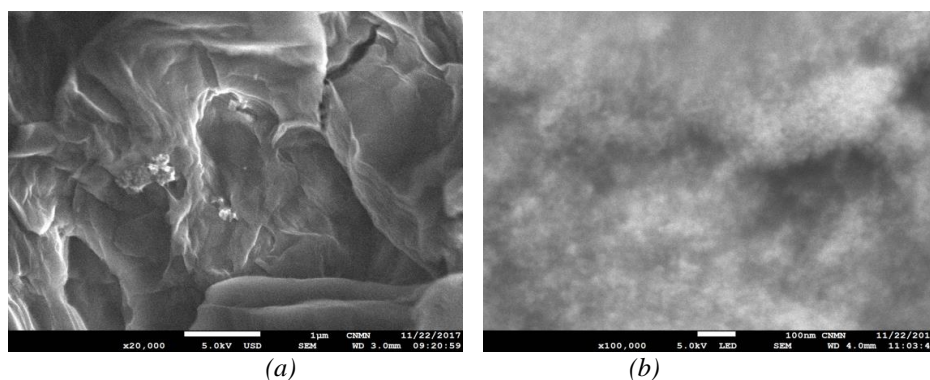


Fig. 2. SEM micrography of a) GO and b) ZnO.

Fig. 3 a) shows the SEM image of composite 1. The average size of the ZnO nanoparticles was found to be 40 nm. The folds seen at the bottom belong to the GO, indicating the low coverage of ZnO with GO. Fig. 2 b) shows the morphology of GO in composite 2, which has a lobar or floral shape that keeps the two materials together. Fig. 3 c) shows an intermediate coverage, which has a ZnO nanoparticle size of 51 nm, which is approximately 10 nm larger than the particle size of composite 1. The increase in the ZnO content increases the grain size of the ZnO/GO composite 3. This increase in the grain size can be attributed to the accelerated diffusion of atoms, leading to the crystal growth of up to 74 nm in diameter (Fig. 3 d).

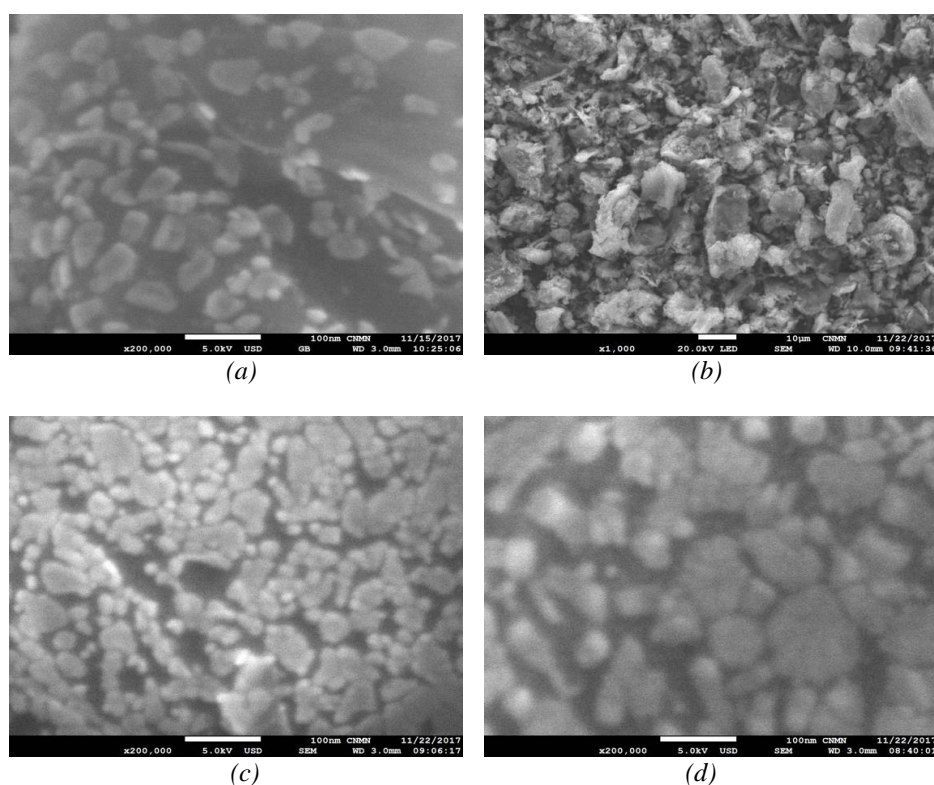


Fig. 3. SEM micrography of a) ZnO/GO composite 1, b)–c) ZnO/GO composite 2, and d) ZnO/GO composite 3.

Fig. 4 a) shows the vibrational modes of GO. Since GO is a carbon-based material, G (Graphite) and D (Disorder) bands are typically observed [28]. The G band located at 1590 cm^{-1} represents the relative degree of graphitization, which assigns the first-order dispersion of the doubly degenerate E_{2g} phonic modes in the center of the Brillouin zone of carbon atoms with sp^2 bonds. The D band located at 1343 cm^{-1} is wider and has higher intensity compared to the G band. This defines the defects in the structures and induced disorders of the vibration modes of the A_{1g} symmetry, which results from the structural imperfections created by the union of the oxygenated groups in the basal plane of carbon during the oxidation of graphite powder [29].

Fig. 4 b) shows the spectra of ZnO/GO composites. Two characteristic bands of ZnO were observed at 330 cm^{-1} and 380 cm^{-1} , corresponding to the coupled vibrational modes E_{2H} – E_{2L} and A_1 (transverse optical, TO), respectively [30]. In addition, the characteristic D and G bands from GO are also observed. Thus, this proves the physical interaction between the zinc oxide nanoparticles on the surface of GO.

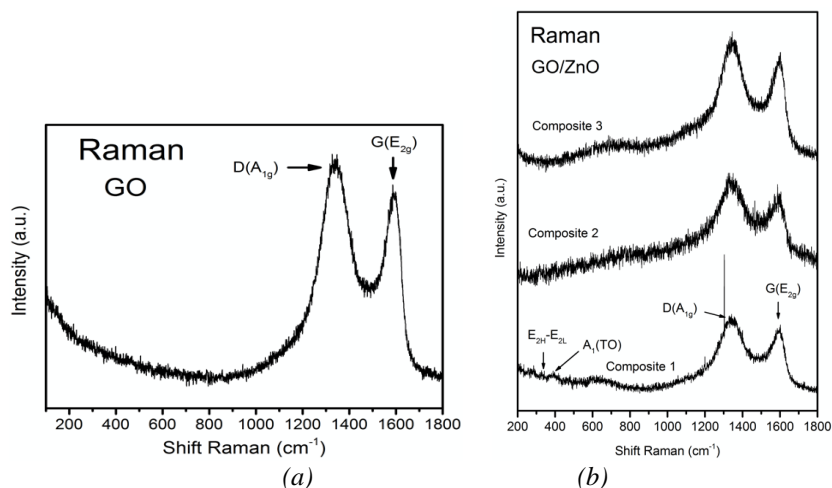


Fig. 4. Raman spectra of a) GO and b) ZnO/GO composites.

Fig. 5 shows the FTIR spectra of GO and ZnO/GO composite 3. These results agree with the Raman characterizations. The bands centered at 1061 cm⁻¹, 1388 cm⁻¹, 1622 cm⁻¹, 1728 cm⁻¹, and 3219 cm⁻¹, correspond to the vibrational modes of C–O–C due to covalent bonds, C–OH due to dipole–dipole interactions, C=C graphite hybridized with sp², C=O from the carboxyl as well as carbonyl groups located on the edges of the GO sheets, and O–H due to the water molecules absorbed in the GO as a result of different electrostatic interactions such as Van der Waals forces, respectively [31], [32].

In the ZnO/GO composite, the intensity of the O–H functional groups decreased. As in the presence of GO, the complete elimination of water is impossible because GO absorbs water from the air. This decrease in the intensity of O–H indicates the reduction of GO. On the other hand, the bands centered in 650 cm⁻¹ and 850 cm⁻¹, corresponding to the vibrational modes Zn–O and C–H, respectively, were observed [33]. The band located at 650 cm⁻¹ corresponds to the E₂ mode of hexagonal ZnO (active Raman), originating from the covalent bonds between Zn⁺ and O⁻ [34]. This indicates that the zinc oxide particles were anchored to the GO sheets.

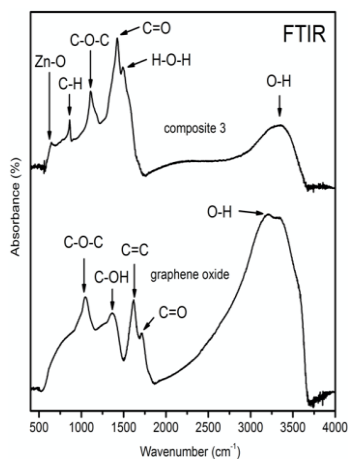


Fig. 5. FTIR spectra of GO and ZnO/GO composite 3.

4. Conclusions

The reduction of GO in ZnO/GO composites has been demonstrated using different characterization techniques. XRD was successfully used to observe the crystal structure of ZnO and the rGO interactions. SEM micrography images revealed that ZnO particles were anchored to

the GO. Furthermore, Raman and FTIR characterizations were used to obtain a perspective of the physics of the developed materials.

This direct and simple synthesis method of zinc oxide and GO composites has been successfully reproduced. Thus, this method is suitable for manufacturing electronic microdevices.

Acknowledgements

The authors of this article are grateful to the Center for Nanoscience and Micro and Nanotechnologies of the IPN for providing characterization equipment for this study. This work was supported by SIP-IPN project 20201241.

References

- [1] J. K. Wassei, R. B. Kaner, *Materials Today* **13**(3), 52 (2010).
- [2] C. Zhao, L. Xing, J. Xiang, L. Cui, J. Jiao, H. Sai, Z. Li, F. Li, *Particuology* **17**, 66 (2014).
- [3] P. Y. Puah, P. Y. Moh, P. C. Lee, S. E. How, *Advanced Performance Materials* **33**(13), 835 (2018).
- [4] S. T. Jadhav, S. J. Rajoba, S.A. Patil, S. H. Han, L. D. Jadhav, *Journal of Electronic Materials* **45**, 379 (2016).
- [5] A. Holm, C. J. Wrasman, K. Kao, A. R. Riscoe, M. Cargnello, C. W. Frank, *ACS Publications* **34**(33), 9683 (2018).
- [6] W. ZL, *J Phys Condens Mater* **16**, 829 (2004).
- [7] Ü. Özgür, Y. I. Alivov, C. Liu, A. Teke, M. A. Reshchikov, S. Doğan, V. Avrutin, S.-J. Cho, H. Morkoç, *Journal of Applied Physics* **98**(4) (2005).
- [8] K. Edalati, A. Shakiba, J. Vahdati-Khaki, S. M. Zebarjad, *Materials Research Bulletin* **74**, 374 (2016).
- [9] L. Spanhel, M. A. Anderson, *Journal of the American Chemical Society* **113**, 2826 (1991).
- [10] J. N. Hasnidawani, H. N. Azlina, H. Norital, N. N. Bonnia, S. Ratim, E. S. Ali, *Procedia Chemistry* **19**, 211 (2016).
- [11] G. Sharmila, M. Thirumarimurugan, C. Muthukumar, *Microchemical Journal* **145**, 578 (2019).
- [12] R. L. Hoffman, *Journal of Applied Physics* **95**(10), 5813 (2004).
- [13] J. Huang, L. Wang, R. Xu, K. Tang, W. Shi, Y. Xia, *Semiconductor Science and Technology* **24**(7), (2009).
- [14] N. Sekine, C. H. Chou, W. L. Kwan, Y. Yang, *Organic Electronics* **10**(8), 1473 (2009).
- [15] L. Zhu, W. Zeng, *Sensors and Actuators A: Physical* **267**, 242 (2017).
- [16] T. N. Blanton, D. Majumdar, *Power Diffraction* **28**(2), 68 (2013).
- [17] A. Ganguly, S. Sharma, P. Papakonstantinou, J. Hamilton, *American Chemical Society* **115**(34), 17009 (2011).
- [18] D. Yang, A. Velamakanni, G. Bozoklu, S. Park, M. Stoller, R. D. Piner, S. Stankovich, I. Jung, D. A. Field, C. A. Ventrice-Jr, R. S. Ruoff, *Carbon* **47**, 145 (2009).
- [19] A. Garcia-Gallastegui, D. Iruetagoiena, V. Gouvea, M. Mokhtar, A. M. Asiri, S. N. Basahel, S. A. Al-Thabaiti, A. O. Alyoubi, D. Chadwick, M. S. P. Shaffer, *Chemistry of Materials* **24**(23), 4531 (2012).
- [20] J. Lee, N. T. Khoa, S. W. Kim, E. J. Kim, S. H. Hahn, *Materials Chemistry and Physics* **164**, 29 (2015).
- [21] X. Hua, Y. Yu, Y. Wang, J. Zhou, L. Song, *Applied Surface Science* **329**, 83 (2015).
- [22] B. S. Bendre, S. Mahamuni, *JMR* **19**(3), 737 (2004).
- [23] L. J. Cote, R. Cruz-Silva, J. Huang, *Journal of the American Chemical Society* **131**(31), 11027 (2009).
- [24] Z. Q. Li, C. J. Lu, Z. P. Xia, Y. Zhou, Z. Luo, *Carbon* **45**(8), 1686 (2007).
- [25] T. Jan, J. Iqbal, M. Ismail, A. Mahmood, *Journal of Applied Physics* **115**(15), (2014).
- [26] R. B. Kale, *International Journal for Light and Electron Optics* **126**(11-12), 1109 (2015).

- [27] M. F. R. Hanifah, J. Jaafar, M. Aziz, A. F. Ismail, M. H. D. Othman, M. A Rahman, *Bulletin of Materials Science* **38**(6), 1569 (2015).
- [28] G. Dovbeshko, O. Fesenko, A. Dementjev, R. Karpicz, V. Fedorov, O. Y. Posudievsky, *Nanoscale Research Letters* **9**, 1 (2014).
- [29] J. R. Rani, S. I. Oh, Jae-Hyung Jang, *Materials* **8**(12), 8460 (2015).
- [30] T. L. Phan, R. Vincent, D. Cherns, N. X. Nghia, V. V. Ursaki, *Nanotechnology* **19**(47), (2008).
- [31] L. Tan, Y. C. Zhang, B. Wang, H. M. Luo, H. X. Feng, *ChemPlusChem* **79**(4), (2014).
- [32] B. Qi, S. R. Lu, X. E. Xiao, L. L. Pan, F. Z. Tan, J. H. Yu, *Express Polymer Letters* **8**(7), 467 (2014).
- [33] L. Zheng, Y. Zheng, C. Chen, Y. Zhan, X. Lin, Q. Zheng, K. Wei, *ChemPlusChem* **77**(3), 217 (2012).
- [34] Z. Fakhroueian, F. M. Harsini, F. Chalabian, F. Katouzian, A. Shafiekhani, P. Esmailzadeh, *Advances in Nanoparticles* **2**(03), 247 (2013).